

Article

Computational Investigation of Ionization Energies and Absorption Spectra of Metallocenes: Effect of the Metal Center on Electronic Properties

Christina Eleftheria Tzeliou ¹, Konstantinos P. Zois ¹ and Demeter Tzeli ^{1,2,*}

¹ Laboratory of Physical Chemistry, Department of Chemistry, National and Kapodistrian University of Athens, Panepistimiopolis Zografou, 157 84 Athens, Greece; ctzeliou@chem.uoa.gr (C.E.T.); kpzois@chem.uoa.gr (K.P.Z.)

² Theoretical and Physical Chemistry Institute, National Hellenic Research Foundation, 48 Vassileos Constantinou Ave., 116 35 Athens, Greece

* Correspondence: tzeli@chem.uoa.gr; Tel.: +30-210-7274307

Abstract

Since the synthesis of ferrocene in 1951, metallocenes have attracted attention, making the accurate prediction of their electronic structure and ionization energy crucial for understanding their photophysical and electrochemical behavior in materials and in biological systems. Here, we combined Density Functional Theory (DFT), Complete Active Space Self-Consistent Field (CASSCF), NEVPT2 (N-Electron Valence State Perturbation Theory) and Coupled Cluster approaches (CCSD, DLPNO-CCSD(T)) to study the electronic structure, ionization energies (IEs) and absorption spectra of metallocene and metallocenium complexes in the gas phase and in THF implicit solvent. DFT IEs agree closely with NEVPT2 and DLPNO-CCSD(T) values and with experiment values (deviations 0.02–0.3 eV). For CASSCF and NEVPT2, the minimal active space of the d electrons at six orbitals is not enough for the accurate prediction of the IEs, while an extended active space incorporating all 3d metal electrons plus four ligand valence electrons into 15 orbitals improves the calculated IE values. In solution, computed oxidation energies (OEs) in THF reproduce experimental values and follow the Fe > Ni > Co ordering. Substitution of metallocene complexes with chromophore units results in similar OEs. Overall, the substitution effects remain modest: the effect of substitution on OE values results in differences up to 0.2 eV. These results clarify the effect of the metal center on IE and OE values and UV–vis absorption behavior.

Keywords: metallocene; metallocenium; iron; cobalt; nickel; open shell systems; transition metals; DFT; CCSD; DLPNO; CASSCF; absorption spectra; ionization energy

Academic Editor: Liuhua Mu

Received: 14 March 2026

Revised: 22 April 2026

Accepted: 23 April 2026

Published: 30 April 2026

Copyright: © 2026 by the authors. Licensee MDPI, Basel, Switzerland. This article is an open access article distributed under the terms and conditions of the [Creative Commons Attribution \(CC BY\) license](https://creativecommons.org/licenses/by/4.0/).

1. Introduction

Since its first characterization in 1951 [1], ferrocene has been extensively studied [2–13]. In its pure form, it is a highly stable, light-orange crystalline solid whose UV–vis absorption spectrum has been thoroughly investigated [11,14]. Its characteristic color arises from a dipole-forbidden transition at 440 nm and a shoulder at 528 nm, both of which gain intensity through vibronic coupling. Additional weak features include a band at 324 nm and several allowed but low-intensity absorptions between 265 and 230 nm. Very intense absorption appears at wavelengths higher than 202 nm, due to strongly allowed charge transfer (CT).

From a theoretical perspective, both low- and high-lying excited states of ferrocene exhibit comparable degrees of charge-transfer character [2]. Its electronic structure and geometry, in both eclipsed and staggered conformations, have been studied in the gas phase using Density Functional Theory (DFT), Configuration Interaction Singles (CIS), and Time-Dependent DFT (TD-DFT). The calculated vibrational modes for singlet, triplet, and quintet spin states show good agreement with experimental observations [7]. The different oxidation states of metallocenes influence their optical characteristics. For iron, it has been established that neutral ferrocene is essentially apolar, with its ground and low-lying excited states largely insensitive to solvent polarity, whereas the properties of the ferrocenium cation depend significantly on the solvent environment [3]. The redox potential of the ferrocenium/ferrocene (Fc^+/Fc) couple has been successfully reproduced using a combined Molecular Dynamics (MD) and Perturbed Matrix Method (PMM) approach, yielding results consistent with experimental data [3,12,13].

Substitution of the metal center with other transition metals also leads to pronounced changes in color and electronic properties. While ferrocene is orange, cobaltocene forms deep-purple crystals and nickelocene appears as a bright-green solid [14]. Compared to ferrocene, these analogs have been studied less extensively. In the gas phase, their valence electronic structure has been probed using photoelectron spectroscopy [15], allowing assignment of calculated shape resonances to specific initial and final states. For nickelocene, absorption maxima have been reported at 192, 307.5, and 692 nm, with additional shoulders at 270, 345, 440, and 570 nm [4]. The transition at 192 nm is allowed but less intense than the corresponding transition in ferrocene, while the band at 307.5 nm is relatively strong and occurs near the wavelength of the intermolecular charge-transfer band of ferrocene in carbon tetrachloride. The remaining features closely parallel those observed in ferrocene [4]. Analysis of the electronic structure of the three metallocenes shows that their valence molecular orbitals arise from combinations of metal and cyclopentadienyl (Cp) atomic orbitals [10,16]. Comparative studies indicate that cobaltocene is more stable than nickelocene. Far-UV absorption spectra recorded in the gas phase reveal that charge-transfer states possess partial Rydberg character, although contributions from higher electronic configurations cannot be neglected [5].

The redox properties of metallocenes have likewise been studied in detail. Reduction potentials for the M^0/M^+ couples ($\text{M} = \text{Fe}^{2+}/3+, \text{Co}^{2+}/3+, \text{Ni}^{2+}/3+$) range from 4.85 to 5.25 V in water and acetonitrile [8], and gas-phase values have also been computed, all in good agreement with experimental data [17–25].

More specifically, Rudshiteyn et al. [18] applied the auxiliary-field quantum Monte Carlo, where the adiabatic ionization energy was computed with the two-step procedure (AFQMC CS), or directly as a two-point energy difference (AFQMC PC) in six metallocene complexes to calculate IEs theoretically. They also carried out DFT calculations using various functionals along with one variant of localized Coupled Cluster calculations (DLPNO-CCSD(T_0)) with moderate PNO cut-offs). They evaluated the mean absolute errors and by utilizing experimental solvation energies, they showed that accurate reduction potentials in solution for the metallocene series can be obtained from the AFQMC gas-phase results.

Aðalsteinsson and Bjornsson [22] assessed the accuracy of DLPNO-CCSD(T) with respect to geometry, reference determinant, basis set size and extrapolation schemes, PNO cut-off and extrapolation, local triples approximation, relativistic effects and core–valence correlation using highly accurate ZEKE-MATI experimental measurements of gas-phase adiabatic and vertical ionization energies of cobaltocene. Results showed that CCSD(T) seems fully capable of describing the IEs of these systems well.

Zhao et al. [8] conducted a theoretical investigation on the accurate reduction potential predictions for ferrocene, cobaltocene and nickelocene. The gas-phase ionization energy was computed with CCSD(T) F12, including the zero-point energy correction, core–

valence electronic correlation, and relativistic and spin–orbit coupling effects. This theoretical procedure was found to yield accurate reduction potential predictions of $\text{Cp}_2\text{Fe}^+/\text{Cp}_2\text{Fe}$, $\text{Cp}_2\text{Co}^+/\text{Cp}_2\text{Co}$ and $\text{Cp}_2\text{Ni}^+/\text{Cp}_2\text{Ni}$ redox couples both in aqueous and non-aqueous media.

Why is theory important? Accurate ab initio prediction of electronic structure, excited states, and ionization energies is essential for understanding the chemical, photophysical, and electrochemical behavior of transition-metal complexes in both materials science and biological contexts [26–28]. With theory we can also assist in the design of new systems without the need to first synthesize them.

In the present study, we employ a range of computational approaches to investigate the metallocene systems $\text{M}^{2+}(\text{C}_5\text{H}_5^-)_2$ and their oxidized counterparts $\text{M}^{3+}(\text{C}_5\text{H}_5^-)_2$ (Mc and Mc^+ , with $\text{M} = \text{Fe}, \text{Co}, \text{Ni}$). This includes DFT, Complete Active Space Self-Consistent Field (CASSCF), Coupled Cluster (CC), and Domain-Based Local Pair Natural Orbital CC (DLPNO-CC). The calculations are performed in gas phase and in solution by employing a polarizable continuum model (PCM). The performance of DFT, DLPNO-CCSD(T), CASSCF, and NEVPT2 is assessed by comparison of our results with available experimental data. Note that multireference methods have not been applied to such systems so far, to our knowledge. So, while DFT and DLPNO-CCSD(T) are commonly used methodologies for ionization potentials, multireference treatments of oxidized metallocenes and metalloceniums remain underexplored. Therefore, the methodologies employed here provide a comprehensive assessment that takes into consideration both advantages and limitations of each approach to obtain reliable and well-balanced results. Furthermore, application of the above methodologies is also shown for exemplary metallocene-containing chromophores. Thus, the aim is to develop systematic linkages between metal identity, oxidation energies in solution, and absorption properties of both metallocenes and their derivatized analogs. The comparison between gas-phase ionization energies and solution-phase oxidation energies, along with CCSD benchmarking and spin-state effects analysis in nickel complexes, provides further insight into the effect of derivatization on the electronic structure of metallocene units.

2. Results and Discussion

First, we present our data on ferrocene (Fc), ferrocenium (Fc^+), cobaltocene (Cc), cobaltocenium (Cc^+), nickelocene (Nc), and nickelocenium (Nc^+), see Figure 1, in the gas phase and in THF solvent. We studied the ground and excited states in the gas phase via (TD-)DFT, DLPNO-CCSD(T), CASSCF, and NEVPT2 methodologies and we calculated the ionization energy (IE) that corresponds to the reaction $\text{Mc} \rightarrow \text{Mc}^+ + \text{e}^-$. Note that the ionization energy in the gas phase is also called *ionization potential*. Here we use the term ionization energy. Comparison of our results with the experimental and published high-level calculations is presented as well.

Data on the ground states and the absorption spectra of the six species in THF solution upon performing (TD-)DFT calculations are also presented. In solution, the corresponding energy required to oxidize the metallocene, $\text{Mc} \rightarrow \text{Mc}^+ + \text{e}^-$, is called oxidation energy (OE). Note that the oxidation energy is different from the redox potential which measures the relative electrochemical tendency for the reduction, e.g., $\text{A}^+ + \text{e}^- \rightarrow \text{A}$, versus the standard hydrogen electrode, expressed in volts under standard conditions.

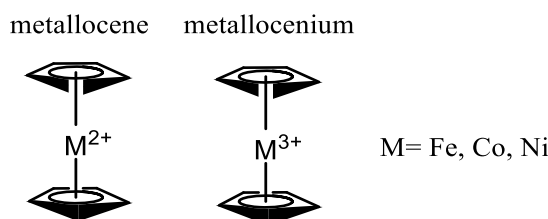


Figure 1. Molecular structures of the metal complexes under study.

DFT: The geometry and electronic spectra of Fc, Cc, Nc, Fc⁺, Cc⁺, and Nc⁺ were calculated via DFT and TD-DFT using the PBE0 [29–31], TPSSh [32,33] and ω B97X-D [34] functionals in conjunction with the 6-31G(d,p) [35] and def2-TZVP [36] basis sets in the gas phase and in THF solvent (see Table S1, SI). Note that the PBE0 functional is widely used and can generally provide geometries and electronic spectra in good agreement with the experiment [37,38]. It has been successfully used in conjunction with the 6-31G(d,p) basis set in our previous calculations on derivatives of ferrocene species [39,40] in excellent agreement with available experimental data regarding the absorption UV–vis spectra [41]. TPSSh is widely used and it has been reported to provide reliable descriptions regarding transition-metal electronic structure and metal–ligand interactions [32,33] and it often improves the balance between exchange and correlation effects opposed to conventional hybrid GGAs [32,33]. Finally, ω B97X-D is a popular functional and is regarded appropriate for the description of long-range interactions [34]. The formulation of ω B97X-D improves the description of long-range electron interactions and reduces self-interaction errors, which are particularly relevant for transition-metal systems and for the prediction of ionization energies and excitation energies [34].

CC: Coupled Cluster Singles and Doubles (CCSD) [42] and DLPNO [43], an efficient local approximation, were employed for the CC calculations, i.e., DLPNO-CCSD and DLPNO-CCSD(T), where the triplet excitations are treated perturbatively. DLPNO makes CC methods practical for large systems since it has the advantage of reducing the computational cost, while retaining near-“gold-standard” accuracy [43].

NEVPT2: CASSCF [44] and NEVPT2 [45,46] calculations were also performed on all metallocene and metallocenium complexes. The CASSCF and NEVPT2 calculations were carried out on geometries obtained at the ω B97X-D/def2-TZVP level of theory, since it has been demonstrated that DFT can provide better geometries for the metal complexes than the CASSCF method [47–49]. The active space is denoted as CASSCF(n,o) and NEVPT2(n,o), respectively, where n refers to the number of electrons and o corresponds to the number of orbitals. Here, two types of active spaces (a) and (b) were used. Specifically, the active spaces are constructed as follows: (a) Fc (6e, 6o), Fc⁺ (5e, 6o), Cc (7e, 6o), Cc⁺ (6e, 6o), Nc (8e, 6o), Nc⁺ (7e, 6o), and (b) Fc (10e, 15o), Fc⁺ (9e, 15o), Cc (11e, 15o), Cc⁺ (10e, 15o), Nc (12e, 15o), and Nc⁺ (11e, 15o); for instance, Fc⁺(5e,6o) means that five electrons are actively distributed within the space of six orbitals. Space (a) has been constructed to include only the metal-centered 3d electrons to six orbitals (there are six sd^5 orbitals of metal) and these are the key ligand-based orbitals involved in bonding and redox processes. Space (b) is an extended active space which has been constructed to include all 3d electrons + four valence occupied electrons of the ligands to 15 orbitals (nine sd^5p^3 orbitals of metal + two occupied orbitals + four unoccupied orbitals).

2.1. Ionization Energy and Electronic Excited States of Metallocene Molecules in Gas Phase

Our calculated adiabatic ionization energies (IEs) of the Fc/Fc⁺, Cc/Cc⁺, and Nc/Nc⁺ species were computed at all levels of theory (see Table 1). The mean absolute errors (MAEs) with respect to the experimental values are also provided. The corresponding

experimental values and the best published extrapolated calculated IEs are also included. Note that at the CASSCF and NEVPT2 levels of theory, the ground states of the species were calculated without any state-average (SA) calculations.

Table 1. Ionization energies (IEs) (eV) using different levels of theory in the gas phase; mean absolute errors (MAEs) with respect to the experimental values; experimental values and the best published extrapolated calculated values are also included.

| Methodology | IE | | | IE ^a | | MAE | |
|-------------------------------------------------------|--------------------|----------------------------------|--------------------|--------------------|--------------------|--------------------|--------------------|
| | Fc/Fc ⁺ | Cc/Cc ⁺ | Nc/Nc ⁺ | Nc/Nc ⁺ | Fc/Fc ⁺ | Cc/Cc ⁺ | Nc/Nc ⁺ |
| PBE0/6-31G(d, p) | 6.24 | 5.12 | 6.21 | 5.14 | −0.40 | −0.24 | −0.03 |
| PBE0/def2-TZVP | 6.37 | 5.46 | 6.55 | 5.52 | −0.27 | 0.11 | 0.32 |
| PBE0/def2-TZVPP | 6.34 | 5.47 | 6.55 | 5.59 | −0.30 | 0.11 | 0.32 |
| ωB97X-D/def2-SVP | 6.53 | 5.47 | 6.61 | 5.47 | −0.11 | 0.11 | 0.38 |
| ωB97X-D/def2-TZVP | 7.16 | 5.44 | 6.56 | 5.57 | 0.52 | 0.09 | 0.32 |
| CASSCF ^b (a) | 4.70 | 5.73 | 6.14 | | −1.94 | 0.38 | −0.10 |
| CASSCF ^c (b) | 5.26 | 5.24 | 5.58 | | −1.38 | −0.12 | −0.66 |
| NEVPT2/def2-TZVP (a) ^b | 5.80 | 4.74 | 5.96 | | −0.84 | −0.62 | −0.28 |
| NEVPT2/def2-TZVP (b) ^c | 6.66 | 5.75 | 6.49 | | 0.02 | 0.40 | 0.26 |
| DLPNO-CCSD/def2-TZVP | 6.45 | 5.31 | 6.73 | 5.48 | −0.19 | −0.05 | 0.50 |
| DLPNO-CCSD(T)/def2-TZVP | 6.46 | 5.02 | 6.31 | 5.29 | −0.18 | −0.34 | 0.07 |
| DLPNO-CCSD/cc-pVTZ | 6.47 | 5.37 | 6.77 | 5.59 | −0.17 | 0.01 | 0.53 |
| DLPNO-CCSD(T)/cc-pVTZ | 6.51 | 5.07 | 6.32 | 5.40 | −0.13 | −0.29 | 0.09 |
| Expt ^d | 6.638 ± 0.065 | 5.355 ± 0.065 5.3275 ± 0.0006 | 6.235 ± 0.065 | | | | |
| Extrapolated-AFQMC PC/CAS ^e | 6.867 ± 0.101 | 5.298 ± 0.080 | 6.222 ± 0.071 | | 0.23 | −0.06 | −0.01 |
| Extrapolated-AFQMC CS/CAS ^e | 6.625 ± 0.088 | 5.392 ± 0.079 | 6.255 ± 0.093 | | −0.01 | 0.04 | 0.02 |
| Extrapolated-DLPNO-CCSD(T) ₀ ^f | 6.772 | 5.308 | 6.393 | | 0.13 | −0.05 | 0.16 |
| CCSD(T) _{Canonical} /cc-pVDZ-DK ^g | | 4.844 | | | | −0.51 | |
| CPS(2)(T ₀)/cc-pVDZ-DK ^h | | 4.863 | | | | −0.49 | |
| Extrapolated CPS ⁱ | | 5.2579 | | | | −0.10 | |
| CCSD(T)-F12 ^j | 6.790 | 5.287 | 6.321 | | | | |

^a With respect to the singlet state of Nc. ^b Type (a) CASSCF and NEVPT2 calculations. ^c Type (b) CASSCF and NEVPT2 calculations. ^d Refs. [20–24]. ^e Ref. [18], auxiliary-field quantum Monte Carlo. ^f Ref. [18], extrapolated values with TZ/QZ basis sets. ^g Ref. [23]. ^h Ref. [22], complete PNO space limit (fS). ⁱ Ref. [22], extrapolation of total ionization energy DLPNO-CCSD(T) energies to complete PNO space limit (CPS), cc-pwCVnZ (Co)/cc-pVnZ (C,H). ^j Ref. [8], CCSD(T)-F12/aug-cc-pVQZ method, where the zero-point energy correction, core–valence electronic correlation, and relativistic and spin–orbit coupling effects are included.

The measurement of the ionization and reduction energies of ferrocene experimentally is resource-intensive, with older reports (1960s–1990s) showing gas-phase ionization energies (IEs) from 6.60 to 7.20 eV, NIST’s benchmark at 6.71 ± 0.08 eV, and via ETE at 6.638 ± 0.065 eV. [21] Experimentally, the adiabatic ionization for cobaltocene has been measured at 5.3275 ± 0.0006 eV (ZEKE-MATI) and 5.355 ± 0.065 eV (ETE), and for nickelocene at 6.235 ± 0.065 eV (ETE) [20,23,24].

Here, we calculate the IEs of Fc/Fc⁺, Cc/Cc⁺, and Nc/Nc⁺ with the commonly used PBE0 functional for the calculation of the UV–vis spectra [38,39] and the ωB97X-D functional which is a good choice since it can describe long-range interactions. Our results are in good agreement with the experimental results (see Figure 2). Specifically, the deviation of the DFT-calculated IE values from the experimental ones ranges from 0.03 eV to 0.52 eV, supporting the reliability of the spectral assignments. The commonly used PBE0/6-

31G(d,p) method, which is applied for the calculation of the electronic spectra of large complexes, predicts the IP values very well, with an error that ranges from 0.5% (Nc/Nc⁺) to 6% (Fc/Fc⁺).

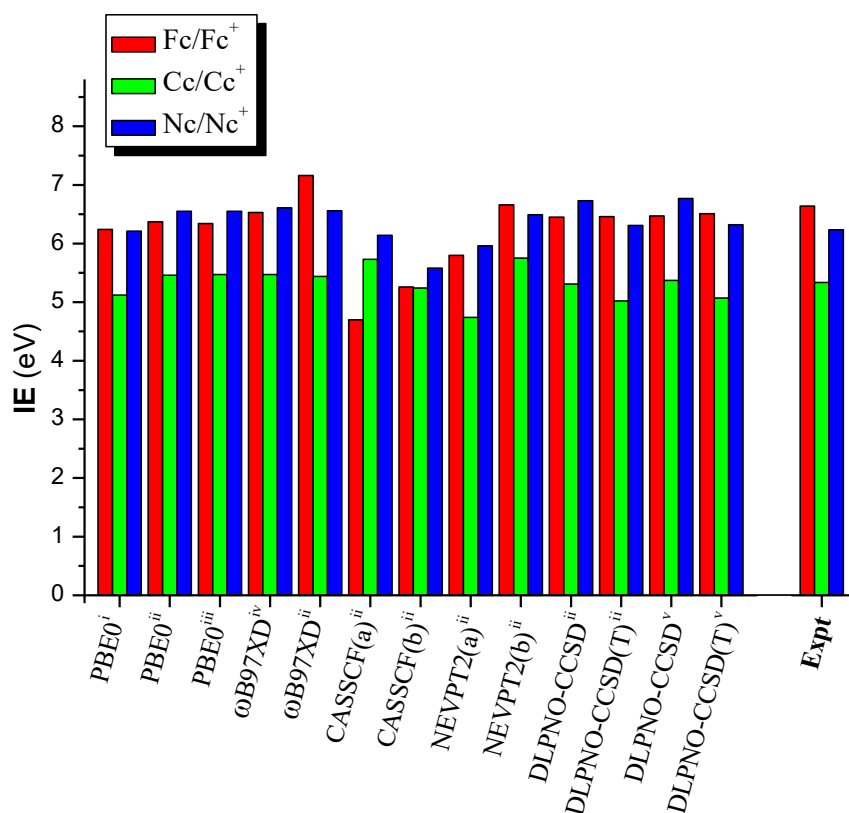


Figure 2. Ionization energies (IEs) of Fc/Fc⁺, Cc/Cc⁺, and Nc/Nc⁺ at different levels of theory in the gas phase, where i: 6-31G(d, p), ii: def2-TZVP, iii: def2-TZVPP, iv: def2SVP, and v: cc-pVTZ. Experimental values are given for comparison [20,23,24]. (a) stands for Type (a) CASSCF and NEVPT2 calculations and (b) for Type (b) CASSCF and NEVPT2 calculations, as stated above.

Furthermore, the NEVPT2 methodology was applied using two active spaces NEVPT2(5e–8e,6o) and NEVPT2(9e–12e,15o). The deviation of the NEVPT2-calculated IE values from the experimental ones ranges from 0.28 eV to 0.84 eV in the small active space, while increase in the active space leads to a decrease in the deviation, i.e., the deviation from the experimental values ranges from 0.02 eV to 0.26 eV. So, our best NEVPT2 IE values are 6.66 eV (Fc/Fc⁺), 5.75 eV (Cc/Cc⁺), and 6.49 eV (Nc/Nc⁺). Overall, the extended active space (b) results in IEs that are in better agreement with the experimental values than the minimal active space (a) for both CASSCF and NEVPT2 methods. So, the active space of the d electrons at six orbitals is not enough for the accurate prediction of the IEs. Finally, it should be noted that overall CASSCF provides less accurate IE data than DFT results even though a large active space is used.

DLPNO-CCSD(T) using a triple zeta quality basis set predicts the IP values very well, i.e., 6.51 eV, 5.07 eV and 6.32 eV, respectively. The largest DLPNO-CCSD(T) deviation is observed for the Cc/Cc⁺ pair; however, the corresponding DLPNO-CCSD value is 5.37 eV in excellent agreement with the experimental one of 5.355 ± 0.065 eV, but it most probably is due to some spurious cancellation of errors. In general, DLPNO-CCSD(T) can handle small amounts of static correlation very well. On the other hand, the NEVPT2 method should be employed when the multireference treatment of a system is necessary, so that both static and dynamic correlation are included. The issue of the NEVPT2 method is that it is affected by the active spaces chosen [50] which is observed here as well, especially in

the case of the Fc/Fc⁺ pair. In general, our results are in very good agreement with recent theoretically calculated IEs using the auxiliary-field quantum Monte Carlo [18] where the adiabatic ionization energy is computed with the two-step procedure (AFQMC CS), or directly as a two-point energy difference (AFQMC PC) [18]. This is supported by the mean absolute error values as seen in Table 1. Furthermore, their AFQMC-calculated IEs were extrapolated as well as at DLPNO-CCSD(T₀) with TZ/QZ basis sets [19] or DLPNO-CCSD(T) energies to complete PNO space limit (CPS) using cc-pwCVnZ (Co)/cc-pVnZ (C,H) [22]. The extrapolation reduced the deviation from the experimental values, and the calculated deviation ranges from 0.01 eV to 0.16 eV, showing the extrapolation is necessary for excellent agreement with the experimental values. The extrapolation shows that the methods can provide excellent results; however, when large complexes or molecular systems including metallocenes are calculated, the extrapolation of the IE values is obviously not feasible. A two-point extrapolation based on DZ/TZ basis sets may be used, but double- ζ quality is not recommended for CCSD(T). The present calculations show that commonly used density functionals such as PBE0 and ω B97X-D can provide good energetics at reduced computational cost, while NEVPT2 and DLPNO-CCSD(T) are expected to yield consistently good results in more complex systems where DFT may fail, but with a significantly increased cost in computational resources.

The relative energies of Fc/Fc⁺, Cc/Cc⁺, and Nc/Nc⁺ via (TD-)DFT, DLPNO-CCSD(T), CASSCF, and NEVPT2 methodologies are depicted in Figure 3. At the CASSCF and NEVPT2 levels of theory, the excited states were calculated via state-average (SA) calculations including 10 states for each multiplicity of spin, i.e., Fc: singlet, triplet, and quintet states; Fc⁺: doublet, quartet, and sextet states; Cc: doublet and quartet states; Cc⁺: singlet, triplet, and quintet states; Nc: singlet and triplet; and Nc⁺: doublet and quartet. The ground state of ferrocene is a singlet closed shell state. The first excited state is a triplet state lying at 1.44(1.56)[2.24] eV at PBE0(CASSCF)[NEVPT2]. The lowest-in-energy quintet state lays at (2.53)[3.40] eV respectively; it is observed that the NEVPT2 relative energy gaps are increased with respect to CASSCF or DFT gaps. The ground state of ferrocenium is a doublet state lying at 6.37(5.26)[6.66] eV above the ground state of ferrocene, while its first excited state is also a doublet state which is energetically degenerate with the ground state of ferrocenium.

Regarding cobaltocene, the state lowest in energy is a doublet state. The first excited state is also a doublet state lying at 0.45(0.53)[0.49] eV, i.e., all methodologies predict the same energy gap, while the quartet state of cobaltocene lays at 0.70(0.92)[0.61] eV above the ground doublet state. The ground state of cobaltocenium is a singlet state lying at 5.46(5.24)[5.75] eV above the ground state of cobaltocene, while the first excited state is a triplet state lying at 1.89(1.81)[4.62] eV above the ground state of cobaltocenium.

Finally, regarding the nickelocene and nickelocenium pair, see Figure 3iii, the state lowest in energy of nickelocene is a triplet state. PBE0 and NEVPT2 predict a singlet state as the first excited state, while CASSCF predicts a triplet state as the ground one. Thus, the lowest triplet state lays at 1.03(1.33)[1.60] eV and it is energetically degenerate with respect to another triplet state, while the first excited singlet state is lying at 1.70(1.02)[1.96] eV and is also energetically degenerate to another singlet one. Overall, PBE0 is in better agreement with respect to the IEs compared to the CASSCF.

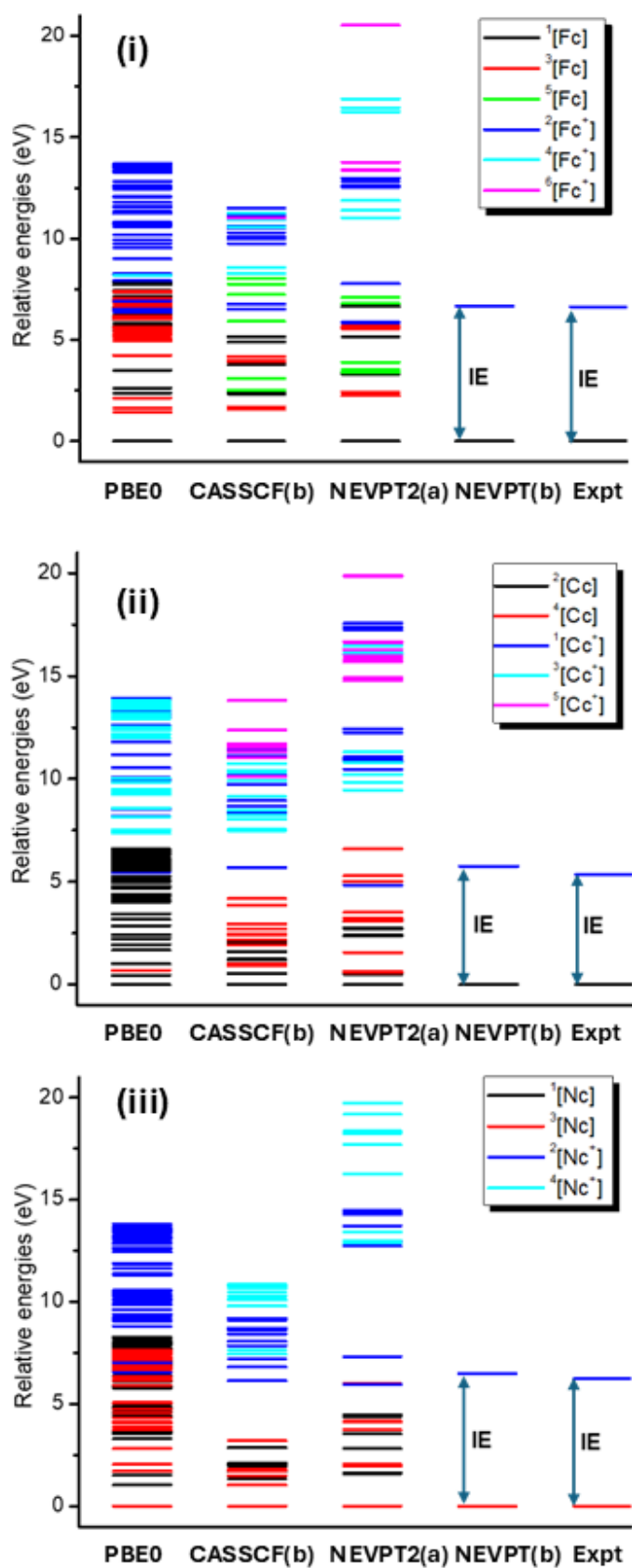


Figure 3. Relative energies of the electronic excited states of (i) ferrocene and ferrocenium, (ii) cobaltocene and cobaltocenium, and (iii) nickelocene and nickelocenium via the PBE0/def2-TZVP, CASSCF(b)/def2-TZVP, NEVPT2(a)/def2-TZVP, and NEVPT2(b)/def2-TZVP methods.

2.2. Metallocene Molecules and Derivatives in Implicit Solvent

The metallocene (Fc, Cc, Nc) and metallocenium (Fc⁺, Cc⁺, Nc⁺) molecules have been studied using DFT methodologies in implicit THF solvent. Geometry, oxidation energy and UV-vis absorption spectra have been calculated. These calculated data are compared with those of the metallocene-4-amino-1,8-naphthal-imide-piperazine molecules (1-M²⁺), its protonated complex (1-H⁺-M²⁺), and the corresponding metallocenium complexes from Ref. [39]. The aim is to study the effect of the electronic properties and ionization energy of Mc/Mc⁺ upon derivatization (see Figure 4). Our previous study [41] was focused on the photophysical properties and the effect of structural factors on their absorption spectra as well as the methodologies used for the investigation [41]. Here, these systems are reconsidered within a different framework, while additional states for the nickelocene derivatives have been calculated. Specifically, the triplet states of 1-Ni²⁺ and 1-H⁺-Ni²⁺ were not studied in our previous work and are investigated here. Furthermore, the OEs of the Mc/Mc⁺ are compared with those of their 4-amino-1,8-naphthalimide-piperazine derivatives to determine whether the OEs remain unchanged or are affected by derivatization. To sum up, our aim is to develop systematic linkages between metal identity, oxidation energies in solution, and absorption properties of both metallocenes and their derivatized analogs.

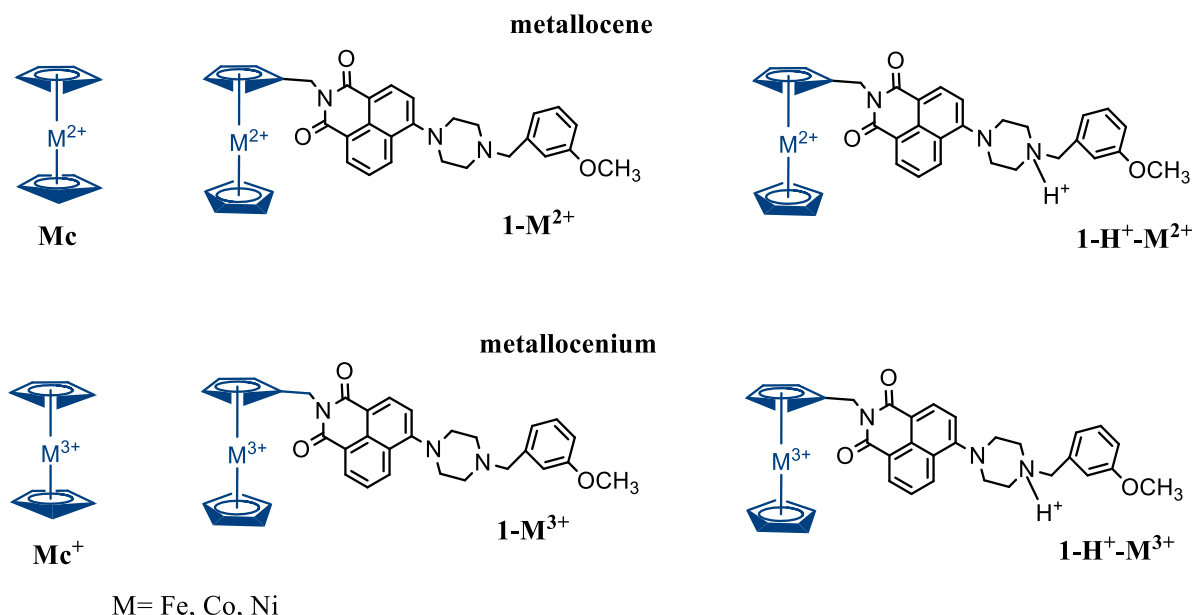


Figure 4. Molecular structures of metal complexes studied in solvent.

2.2.1. Geometry

Regarding the distance of Fe, Ni and Co from the center of each cyclopentadienyl ring in the ferrocene, cobaltocene, and nickelocene complexes, respectively, similar results are obtained with any of the PBE0, TPSSh and ω B97X-D functionals (see Table 2). Specifically, the distances between the metal cation and the center of each cyclopentadienyl ring are increased when Fe²⁺ is oxidized in Fc, 1-M²⁺, and 1-H⁺-M²⁺; however, the increase in the R distances in 1-M²⁺ and 1-H⁺-M²⁺ is smaller than that of ferrocene. For cobaltocene and nickelocene, oxidation leads to a decrease in the distance in most complexes.

Table 2. The distance R (Å) between the metal cation and the center of each cyclopentadienyl ring in the metallocene unit (average values) in implicit THF via the PBE0, TPSSh, and ω B97X-D/6-31G(d,p) methods.

| Species | PBE0 | TPSSh | ω B97X-D | PBE0 | TPSSh | ω B97X-D | PBE0 | TPSSh | ω B97X-D |
|-----------------|-----------------|-------|-----------------|--------------------|--------------------|--------------------|----------------------------------|--------------------|--------------------|
| | Mc ^a | | | 1-M ^b | | | 1-H ⁺ -M ^b | | |
| Fc | 1.584 | 1.596 | 1.562 | 1.623 | 1.613 | 1.632 | 1.621 | 1.613 | 1.631 |
| Fc ⁺ | 1.619 | 1.756 | 1.612 | 1.642 | 1.637 | 1.645 | 1.642 | 1.681 | 1.645 |
| Cc | 1.625 | 1.766 | 1.639 | 1.695 | 1.664 | 1.717 | 1.610 | 1.661 | 1.615 |
| Cc ⁺ | 1.585 | 1.767 | 1.651 | 1.610 | 1.606 | 1.616 | 1.610 | 1.606 | 1.616 |
| ³ Nc | 1.808 | 1.741 | 1.654 | 1.657 ^a | 1.759 ^a | 1.791 ^a | 1.680 ^a | 1.653 ^a | 1.911 ^a |
| ¹ Nc | 1.766 | 1.756 | 1.707 | 1.756 | 1.755 | 1.781 | 1.658 | 1.809 | 1.796 |
| Nc ⁺ | 1.734 | 1.705 | 1.711 | 1.720 | 1.692 | 1.602 | 1.694 | 1.679 | 1.604 |

^a Present study. ^b Ref. [41].

2.2.2. Oxidation Energy

Ionization energy is a gas-phase property, while the corresponding energy difference associated with the oxidation of the metal in solvent is called oxidation energy (OE). Experimentally, the oxidation energy for Fc/Fc⁺ has been measured at 4.8–5.01 eV depending on the solvent, with the most commonly used experimental value being 4.93 eV. This value has been calculated using the equation-of-motion (EOM-IP-CCSD) and effective fragment potential (EFP) methods obtaining a redox potential of 4.94 eV [17]. For the Cc/Cc⁺ and Nc/Nc⁺ pairs, experimental estimated values of 4.94 eV (Cc/Cc⁺) and 4.25 or 4.50 eV (Nc/Nc⁺) in THF have been proposed based on the *redox potential* ($E_{1/2}$) [51]. It should be noted that typically the theoretical calculation of oxidation energy follows a thermodynamic cycle that connects gas-phase electronic energies to solvation effects, where the IE in the solvent is calculated from the gas-phase IE and solvation energies of the oxidized/reduced species. The solution structures of both reduced and oxidized forms of the complexes can be used to reevaluate the reorganization oxidation energy within the linear response approximation [17]. In the present study, the oxidation energy corresponds to a PCM-corrected electronic oxidation energy. Thus, the results provide a good approximation of the experimental OE but are generally qualitative and represent model-dependent energetic trends.

The calculated energy differences of Fc/Fc⁺, Cc/Cc⁺, and Nc/Nc⁺ via DFT and CCSD methods in THF solvent are given in Table 3 and plotted in Figure 5. All DFT functionals used, i.e., PBE0, TPSSh, and ω B97X-D applying two basis sets and the CCSD method, predict similar OE values. Among them, the ω B97X-D functional predicts the largest values, while CCSD predicts the smallest ones.

Table 3. Oxidation energy Mc²⁺ → Mc³⁺ (eV) of the metallocenes and their complexes with PBE0, TPSSh, ω B97X-D, and CCSD in THF solvent.

| | PBE0/ 6-31G(d,p) | TPSSh 6-31G(d,p) | ω B97X-D/ 6-31G(d,p) | CCSD/ 6-31G(d,p) | ω B97X-D/ def2-TZVP | PBE0/ def2-TZVPP | Expt. ^e |
|--------------------------------------------------------------------------------------|---------------------|---------------------|--------------------------------|---------------------|-------------------------------|---------------------|--------------------|
| Fc → Fc ⁺ | 5.31 | 5.38 | 5.44 | 5.29 | 5.56 | 4.77 | 4.94 |
| Cc → Cc ⁺ | 3.50 | 3.19 | 3.49 | 3.21 | 3.41 | 3.85 | 3.60 |
| ³ Nc → Nc ⁺ | 4.59 | 4.20 | 4.62 | 3.89 | 5.01 | 4.95 | 4.50 |
| ¹ Nc → Nc ⁺ | 3.48 | 3.29 | 3.59 | 3.41 | 3.99 | 3.93 | |
| ³ Nc → ¹ Nc ⁺ ^a | 1.11(1.43) | 0.91(1.14) | 1.03(1.37) | 0.48 | 1.01 | 1.03 | |
| 1-Fe ²⁺ → 1-Fe ³⁺ ^b | 5.30 | 5.38 | 5.45 | | | | |
| 1-Fe ²⁺ -H ⁺ → 1-Fe ³⁺ -H ⁺ ^b | 5.45 | 5.62 | 5.66 | | | | |
| 1-Co ²⁺ → 1-Co ³⁺ ^b | 3.49 | 3.17 | 3.48 | | | | |

| | | | |
|-----------------------------------------------------------------------------------------------|------|------|------|
| $1\text{-Co}^{2+}\text{-H}^+ \rightarrow 1\text{-Co}^{3+}\text{-H}^+$ ^b | 3.28 | 3.35 | 3.14 |
| $1\text{-}^3\text{Ni}^{2+} \rightarrow 1\text{-Ni}^{3+}$ ^c | 4.60 | 4.17 | 4.58 |
| $1\text{-}^3\text{Ni}^{2+} \rightarrow 1\text{-}^1\text{Ni}^{2+}$ | 1.06 | 0.80 | 1.01 |
| $1\text{-}^3\text{Ni}^{2+}\text{-H}^+ \rightarrow 1\text{-Ni}^{3+}\text{-H}^+$ ^c | 4.74 | 4.29 | 4.72 |
| $1\text{-}^3\text{Ni}^{2+}\text{-H}^+ \rightarrow 1\text{-}^1\text{Ni}^{2+}\text{-H}^+$ | 1.05 | 0.76 | 0.98 |
| $1\text{-}^1\text{Ni}^{2+} \rightarrow 1\text{-Ni}^{3+}$ ^{b,d} | 3.52 | 3.38 | 3.57 |
| $1\text{-}^1\text{Ni}^{2+}\text{-H}^+ \rightarrow 1\text{-Ni}^{3+}\text{-H}^+$ ^{b,d} | 3.69 | 3.53 | 3.74 |

^a Adiabatic excitation, vertical excitation in parenthesis. Vertical excitation energies were calculated at the optimized ground-state geometry, whereas adiabatic excitation energies were obtained as the energy difference between optimized ground- and excited-state geometries. ^b Ref. [41]. ^c 1-Ni^{2+} and $1\text{-H}^+\text{-Ni}^{2+}$ at the ground $^3\text{A}_1$ state. ^d 1-Ni^{2+} and $1\text{-H}^+\text{-Ni}^{2+}$ at $^1\text{A}_1$ state. ^e In the present study, the OEs correspond to PCM-corrected electronic oxidation energies which provides a good approximation of the experimental OEs.

The Fc/Fc⁺ units and complexes present the highest oxidation energies of the three transition metals under study, while the Cc/Cc⁺ units and complexes present the lowest oxidation energies both theoretically and experimentally. Comparison of our theoretical oxidation energy values of all three functionals with the experimental ones shows that PBE0 is the best overall. The best results for the oxidation energy of Fc and 1-Fe^{2+} are 5.31 eV and 5.30 eV, respectively, whereas, for the protonated complexes, it is increased to 5.45 eV. The oxidation energies for Co and Ni complexes were smaller. For Cc and 1-Co^{2+} the oxidation energies are 3.50 eV and 3.49 eV, respectively, while for the protonated complexes it is decreased to 3.28 eV. For the nickel complexes at their ground state, the oxidation energies of ^3Nc and $1\text{-}^3\text{Ni}^{2+}$ are 4.59 eV and 4.60 eV, respectively, whereas, for the protonated complexes, it increased to 4.74 eV. However, the corresponding oxidation energies for the nickel complexes lying in their singlet excited state are 3.48 eV, 3.52 eV and 3.69 eV, respectively. Note that the triplet–singlet energy difference in the substituted complexes is about 1 eV. Thus, when nickel complexes are in their ground state, their oxidation energy is higher than the corresponding value of cobalt complexes and smaller than that of iron complexes. On the contrary, the corresponding oxidation energies from the singlet states of the nickel complexes are similar to those of the cobalt complexes.

The oxidation energies (OEs) of the metallocene (Fc, Cc, Nc), metallocene-4-amino-1,8-naphthalimide-piperazine molecules (1-M^{2+}), and its protonated complex ($1\text{-H}^+\text{-M}^{2+}$) at various methodologies in THF solvent are plotted in Figure 5. It is shown that the substitution of metallocene slightly influences the oxidation energy, the largest effect observed for the protonated complexes, up to 0.2 eV (see Figure 5a–d). Furthermore, apart from the cobaltocene complexes, protonation increases the oxidation energy, which is consistent with the increase in the metal charge. Finally, comparing the calculated IEs of the metallocene with the OE values, we observe that the OE values are about ~15% (Fc), ~30% (Cc) and 10% (Nc) less than the corresponding IE values.

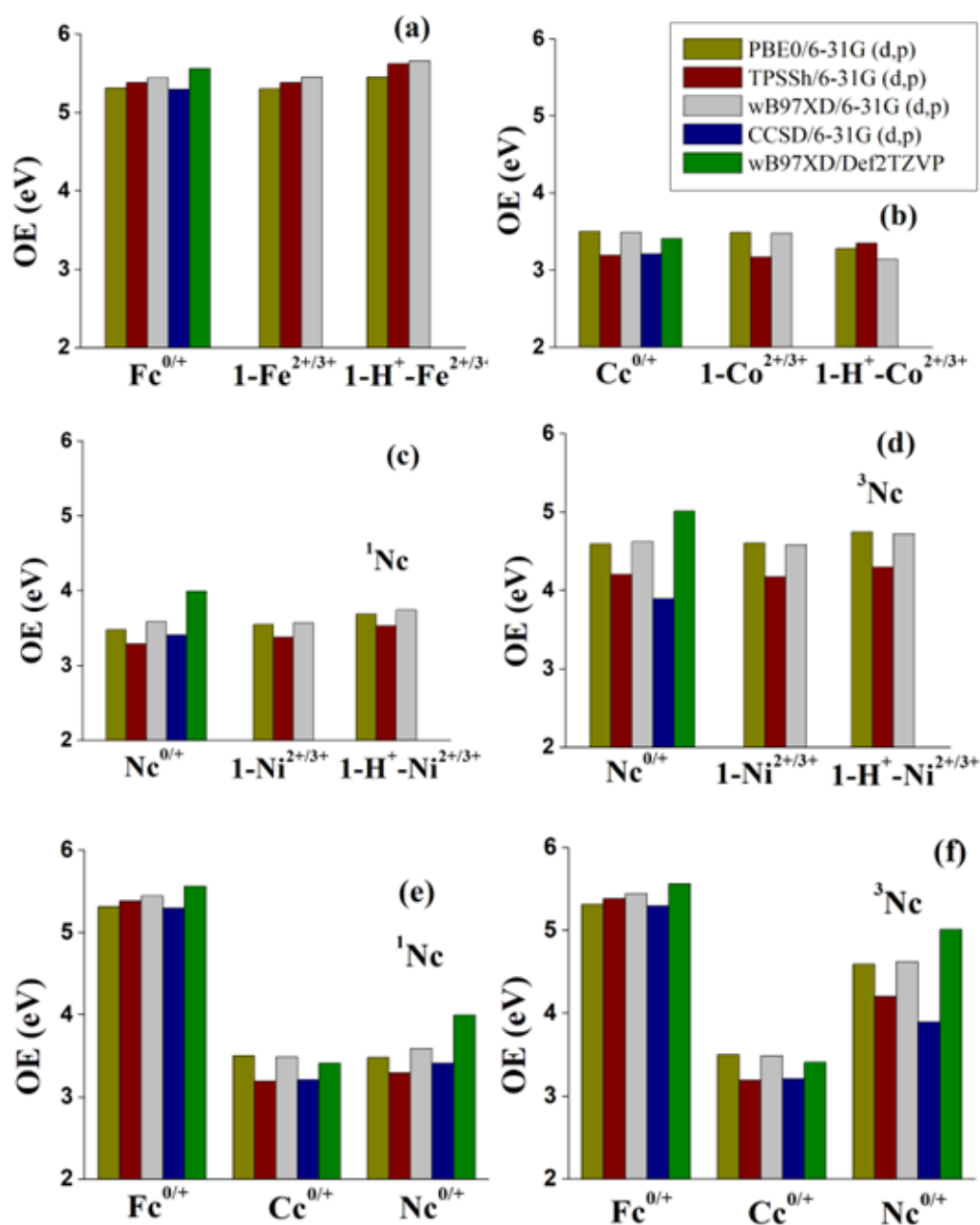


Figure 5. Oxidation energies (OEs) of the metallocene (Fc, Cc, Nc) and metallocene-4-amino-1,8-naphthalimide-piperazine molecules (1-M²⁺) and its protonated complex (1-H⁺-M²⁺) via various methodologies in THF solvent. (a) OEs of Fe²⁺ complexes (b) OEs of Co²⁺ complexes (c) OEs of ¹Ni complexes (d) OEs of ³Ni complexes (e) OEs of the metalloenes including singlet states of Ni²⁺ complexes (f) OEs of the metalloenes including triplet states of Ni²⁺ complexes.

2.2.3. Absorption Spectra

TD-DFT (PBE0, TPSSh, and ω B97X-D) calculations were carried out with the 6-31G(d,p) and def2-TZVP basis sets to study the excited states. It should be noted that the 6-31G(d,p) basis set is a rather small basis set for the small calculated species of twenty-one atoms; however, it is commonly applied in large molecular systems. Previous studies [40,52,53] showed that this basis set is furnished with a balanced and computationally efficient description of the corresponding excited states. The three exchange–correlation functionals (PBE0, TPSSh, and ω B97X-D) used here assist in evaluating the validity of the predicted spectral trends with respect to the functional choice.

The absorption spectra of the metallocene and metallocenium molecules in implicit THF are plotted in Figure 6. The spectra obtained using the PBE0, TPSSh and ω B97X-D functionals are similar. The PBE0 and ω B97X-D main peaks in the UV and vis part are in good agreement with each other, while the TPSSh main peaks are red-shifted compared to PBE0. The observed shift in the main UV peaks using ω B97X-D ranges from 0.07 eV to 0.28 eV. It should be pointed out that range-separated hybrid functionals such as ω B97X-D may systematically shift excitation energies compared to experimental values, mostly in cases where localized valence transitions occur [54,55]. As this work highlights relative spectral trends across the metallocenes under investigation, these systematic deviations do not affect the main conclusions of the study. Generally, PBE0 has been proved to provide absorption spectra in good agreement with the experimental ones in complexes including ferrocene groups [37–40]. Comparing the PBE0/6-31G(d,p) and PBE0/def2-TZVP absorption spectra, they present the same general shape; however, the main peaks using the def2-TZVP basis set are red-shifted in most cases. The shifts range from 9 nm to 28 nm. Finally, upon the inclusion of a diffusion basis set, i.e., PBE0/6-31+G(d,p), the main absorption peaks present small shifts up to 10 nm. So, the increase in the basis set from 6-31G(d,p) to def2-TZVP or the inclusion of the diffuse functions leads generally to a red shift in the absorption peaks, i.e., to smaller energy excitations. The PBE0/def2-TZVP method performs well for the tested molecular systems for the calculation of their absorption spectra.

Selected absorption peaks are given in Table 4. PBE0 and ω B97X-D predict that Fc presents peaks with low intensity around 200 nm and a very intense peak at 175 nm, while for Fc⁺ the corresponding peaks are around 300 nm and 220 nm, respectively, and the intensity of the main UV peak is less intense compared to Fc. Cc presents UV peaks at 300 nm, 240 nm and 210 nm, while Cc⁺ presents an intense peak at 212 nm and a double peak around 150 nm (see Figure 6). Finally, Nc presents UV peaks at 275 nm, while Nc⁺ presents an intense peak at 269. Since the main excitations have a coefficient significantly smaller than 1, the corresponding natural transition orbitals (NTOs) were plotted (see Figure 7). The corresponding frontier orbitals present electron density in both metal and ligands (d-d transitions), except the main peak at 178 nm (Fc) and 229 nm (Fc⁺) where the electron density in the excited NTO is located at the ligands. So, these transitions have a metal-to-ligand charge transfer (MLCT) character (see Figure 7).

Finally, it should be noted that Mc UV–vis bands correspond to metal-to-ligand charge transfer (MLCT) or d-d transitions. Photoexcitation of Mc results in populating the MLCT and d-d states. Optical excitations and ionization processes correspond to distinct physical phenomena. However, in the presence of suitable electron acceptors photoinduced charge transfer can lead to oxidation.

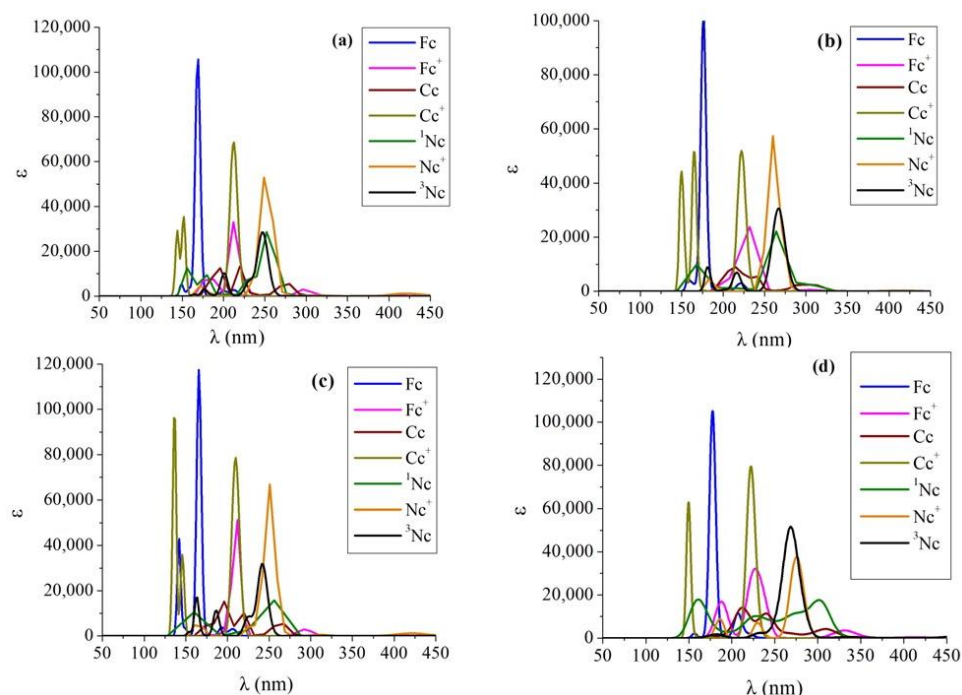


Figure 6. Absorption spectrum of the calculated minimum metallocene and metallocenium structures with (a) PBE0/6-31G(d, p), (b) TPSSh/6-31G(d, p), (c) ω B97X-D/6-31G(d, p), and (d) PBE0/def2-TZVP in implicit THF solvent.

Table 4. Main and first electronic absorption peaks, λ (nm), energy differences ΔE (eV), f -values, and corresponding main excitations of the absorption spectrum of the calculated minimum structures at the PBE0, TPSSh, ω B97X-D/6-31G(d,p) and PBE0/def2-TZVP levels of theory in THF solvent.

| Mol. | Type | PBE0 | | | | TPSSh | | | | ω B97X-D | | | | PBE0/def2tzvp | | | |
|-----------------|-------------------|-----------|------------|-------|--------------------------------------------|-----------|------------|-------|--|-----------------|------------|-------|--|---------------|------------|-------|--|
| | | λ | ΔE | f | Main Excitation | λ | ΔE | f | | λ | ΔE | f | | λ | ΔE | f | |
| Fc | S \rightarrow T | 740.7 | 1.67 | 0.000 | 0.69 H \rightarrow L> | 573.9 | 2.16 | 0.000 | | 737.1 | 1.68 | 0.000 | | 868.2 | 1.43 | 0.000 | |
| | S \rightarrow S | 476.0 | 2.61 | 0.000 | 0.68 H \rightarrow L> | 410.0 | 3.02 | 0.000 | | 502.7 | 2.47 | 0.000 | | 523.4 | 2.37 | 0.000 | |
| | S \rightarrow S | 168.8 | 7.35 | 1.187 | 0.66 H \rightarrow L+5> | 176.4 | 7.03 | 1.089 | | 165.8 | 7.48 | 1.309 | | 177.5 | 6.99 | 1.303 | |
| Fc ⁺ | D \rightarrow D | 215.0 | 5.77 | 0.440 | 0.54 H-3 β \rightarrow L β > | 230.5 | 5.38 | 0.273 | | 210.5 | 5.89 | 0.599 | | 228.8 | 5.42 | 0.662 | |
| Cc | D \rightarrow D | 583.4 | 2.13 | 0.001 | 0.38 H β \rightarrow L β > | 684.6 | 1.81 | 0.000 | | 593.8 | 2.09 | 0.000 | | 636.8 | 1.95 | 0.000 | |
| | D \rightarrow D | 220.7 | 5.62 | 0.136 | 0.87 H-5 β \rightarrow S β > | 219.9 | 5.64 | 0.092 | | 193.5 | 6.41 | 0.194 | | 209.2 | 5.93 | 0.253 | |
| Cc ⁺ | S \rightarrow T | 296.2 | 4.19 | 0.000 | 0.92 H \rightarrow L> | 518.2 | 2.39 | 0.000 | | 286.3 | 4.33 | 0.000 | | 315.1 | 3.94 | 0.000 | |
| | S \rightarrow S | 212.2 | 5.84 | 0.769 | 0.63 H \rightarrow L> | 222.2 | 5.58 | 0.578 | | 209.8 | 5.91 | 0.876 | | 222.2 | 5.58 | 0.899 | |
| ¹ Nc | S \rightarrow S | 253.9 | 4.88 | 0.262 | 0.78 H-3 \rightarrow L> | 268.5 | 4.62 | 0.203 | | 240.1 | 5.16 | 0.281 | | 299.6 | 4.14 | 0.279 | |
| ³ Nc | T \rightarrow S | 868.0 | 1.43 | 0.000 | 0.96 H \rightarrow L> | 1088.2 | 1.14 | 0.000 | | 908.2 | 1.37 | 0.000 | | 727.5 | 1.70 | 0.000 | |
| | T \rightarrow T | 247.4 | 5.01 | 0.318 | 0.97 H-1 \rightarrow L+1> | 267.7 | 4.63 | 0.300 | | 241.9 | 5.13 | 0.356 | | 275.4 | 4.50 | 0.421 | |
| Nc ⁺ | D \rightarrow D | 421.4 | 2.94 | 0.013 | 0.84 H β \rightarrow L β > | 411.9 | 3.01 | 0.003 | | 420.2 | 2.95 | 0.014 | | 480.9 | 2.58 | 0.011 | |
| | D \rightarrow D | 252.6 | 4.91 | 0.669 | 0.83 H-1 β \rightarrow L β > | 259.2 | 4.78 | 0.501 | | 250.4 | 4.95 | 0.745 | | 268.6 | 4.62 | 0.751 | |

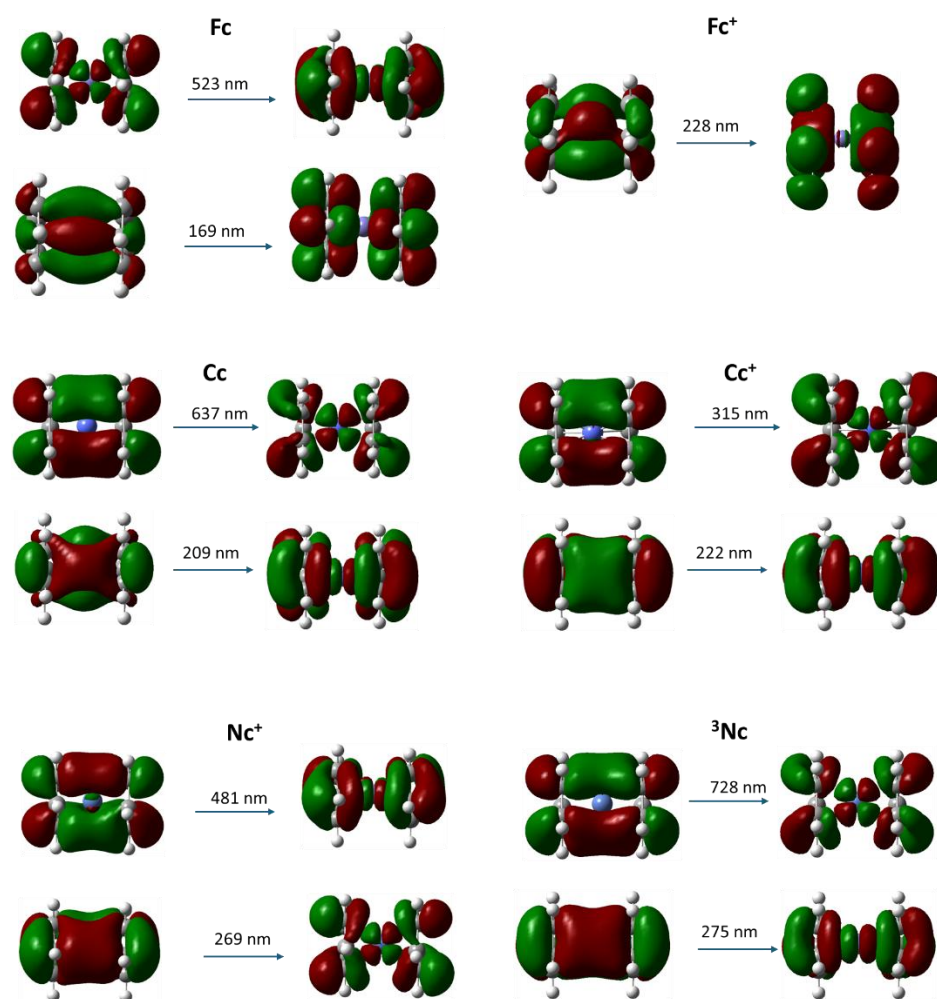


Figure 7. NTO of selected absorption peaks of the metallocene and metallocenium via the PBE0/def2-TZVP method in THF solvent.

3. Methods

The geometry and electronic spectra of ferrocene (Fc), cobaltocene (Cc) and nickelocene (Nc), as well as their corresponding oxidized cations, i.e., ferrocenium (Fc⁺), cobaltocenium (Cc⁺) and nickelocenium (Nc⁺), were calculated via DFT and TD-DFT using the PBE0 [29–31], TPSSh [32,33] and ω B97X-D [34] functionals in conjunction with the 6-31G(d,p) [35] and def2-TZVP [36] basis sets in gas phase and in tetrahydrofuran (THF) solvent for enabling comparison between different levels of theory.

For the DFT level of theory, conformational analyses were carried out for all six complexes in both gas phase and THF solvent. The solvent was included employing the polarized continuum model (PCM) [56]. In metallocene systems, nonspecific electrostatic interactions (e.g., dielectric screening and polarization) often dominate solvent effects due to the sandwich structure the molecules present along with charge distribution, making implicit models like PCM suitable for bulk solvent descriptions. PCM provides a reasonable approximation for trends in ionization energies and excitation energies as these properties are less sensitive to specific solute–solvent hydrogen bonding or short-range effects prevalent in polar or protic solvents [57].

Furthermore, TD-DFT was used to calculate the absorption spectra of the studied structures. In all cases, the absorption spectra of the studied systems were calculated including up to 25 singlet- and 25 triplet-spin excited electronic states. For the excited-state calculations the PBE0, TPSSh, and ω B97X-D functionals in conjunction with the 6-

31G(d,p) basis set were used. Furthermore, the UV–vis absorption spectra of the metallocene/metallocenium species at the PBE0/6-31+G(d,p) and PBE0/def2-TZVP level were calculated for comparison reasons.

Coupled Cluster methodologies were used, i.e., Coupled Cluster Singles and Doubles (CCSD) [42], as well as the Domain-Based Local Pair Natural Orbital Coupled Cluster DLPNO-CC method [43]. DLPNO has the advantage of reducing the computational cost, while retaining near-“gold-standard” accuracy of CC [43]. DLPNO-CCSD and DLPNO-CCSD(T) calculations were carried out in conjunction with the cc-pVTZ [58] basis set.

CASSCF [44] and NEVPT2 [45,46] calculations were also performed on all metallocene and metallocenium complexes using geometries obtained at the ω B97X-D/def2-TZVP level of theory. Two types of active spaces (a) and (b) were used. Active space (a) is the minimal space targeting metal-centered 3d electrons in six sd^5 metal orbitals, while the active space (b) is an extended space incorporating all 3d metal electrons plus 4 ligand valence electrons (total 10–12e) into 15 orbitals (9 sd^5p^3 metal + 2 ligand occupied + 4 unoccupied). Thus, the specific active spaces for Mc/Mc⁺ are as follows: (a): Fc (6e,6o), Fc⁺ (5e,6o), Cc (7e,6o), Cc⁺ (6e,6o), Nc (8e,6o), and Nc⁺ (7e,6o); (b): Fc (10e,15o), Fc⁺ (9e,15o), Cc (11e,15o), Cc⁺ (10e,15o), Nc (12e,15o), and Nc⁺ (11e,15o). So, here, the notation (e.g., Nc⁺ (7e,6o)) indicates 7 electrons distributed across 6 orbitals.

Finally, the Natural Transition Orbitals (NTOs), which are a compact representation of electronic excitations, were plotted for the main absorption peaks.

DFT, TD-DFT and CCSD calculations were carried out using the Gaussian 16 program package [59], while CASSCF, NEVPT2, DLPNO-CCSD, and DLPNO-CCSD(T) were carried out using the ORCA 6.0 software package [60,61].

4. Summary and Conclusions

In this work, we combined DFT, CASSCF/NEVPT2, CCSD and DLPNO-CCSD(T) calculations to study the electronic structure, ionization energies (IEs) and absorption spectra of metallocene and metallocenium complexes (Mc/Mc⁺, where M = Fe²⁺, Co²⁺, and Ni²⁺) in the gas phase and in implicit THF solvent. The effect of the metal ion on the electronic properties and ionization energies of Mc/Mc⁺ and its derivatives was analyzed. The reliability of the methods used is evaluated as well and compared with related benchmarked studies.

Concerning IE, it is found that the DFT methodologies are in good agreement with the computationally expensive NEVPT2 and Coupled Cluster methods as well as the experimental results. For the CASSCF method large active spaces are necessary to predict the IE properly, while for the NEVPT2 method, the extended active space improves the IE values. Thus, for both CASSCF and NEVPT2, the minimal active space of the d electrons at six orbitals is not enough for the accurate prediction of the IEs.

Our best methodologies are NEVPT2(9e–12e,15o) and DLPNO-CCSD(T) which predict 6.66(6.51) eV for the Fc/Fc⁺ pair, 5.75(5.07) eV for Cc/Cc⁺, and 6.49(6.32) eV for Nc/Nc⁺ (CC values in parentheses). Our results are in agreement with the experimental values of 6.638 ± 0.065 eV, 5.355 ± 0.065 eV, and 6.235 ± 0.065 eV, respectively. The mean absolute errors of the calculated values with the experimental ones range from 0.02 eV to 0.3 eV. The largest deviation is observed for the Cc/Cc⁺ pair.

Multireference methods primarily serve as validation tools in this work, while demonstrating that large active spaces are required. Thus, we conclude that inexpensive DFT already provides good agreement with experimental ionization energies, and multireference methods do not significantly alter the observed trend.

In implicit THF, the oxidation energy of metallocene was calculated using DFT and CCSD methods. The ω B97X-D functional predicts the largest values, while CCSD predicts the smallest ones. The oxidation energies (OEs) vary based on the metal center in the parent metallocene, the substituted complexes, and their protonated forms. For the iron

complexes, the neutral species present ΔE s at about 5.30 eV and the protonated forms rise to 5.45 eV. For the cobalt complexes, the corresponding values are about 3.50 eV and 3.28 eV. For the nickel complexes, in the ground state, the corresponding values are 4.59 eV and 4.74 eV and in the singlet state, they are 3.48 eV and 3.69 eV. All in all, the ground-state trend of the oxidation energy is Fe > Ni > Co. For the singlet state of the Ni complexes the OEs are similar to the Co complexes. Overall, substitution slightly affects energies (up to 0.2 eV, largest in protonated forms). Protonation generally raises oxidation energy (except Co), aligning with increased metal charge.

Finally, comparing the calculated IEs of the metallocene with the OEs, it is observed that the OE values are about ~15% (Fc), ~30% (Cc) and 10% (Nc) less than the corresponding IE values.

Supplementary Materials: The following supporting information can be downloaded at <https://www.mdpi.com/article/10.3390/inorganics14050126/s1>. Table S1. Geometries of the calculated minimum structures.

Author Contributions: C.E.T.: investigation, data curation, formal analysis, writing—original draft preparation; K.P.Z.: investigation, data curation; D.T.: conceptualization, methodology, resources, validation, supervision, writing—original draft, writing—review and editing. All authors have read and agreed to the published version of the manuscript.

Funding: CET acknowledges the Hellenic Foundation for Research and Innovation for the financial support of this project under the 5th Call for HFRI PhD Fellowships (Fellowship Number: 21006). KPZ acknowledges the Bodossaki Foundation for the financial support (MSc scholarship 2023–2024).

Institutional Review Board Statement: Not applicable.

Informed Consent Statement: Not applicable.

Data Availability Statement: The original contributions presented in this study are included in the article/Supplementary Materials. Further inquiries can be directed to the corresponding author.

Conflicts of Interest: The authors declare no conflicts of interest.

References

1. Kealy, T.; Pauson, P. A New Type of Organo-Iron Compound. *Nature* **1951**, *168*, 1039–1040.
2. Salzner, U. Quantitatively Correct UV-vis Spectrum of Ferrocene with TDB3LYP. *J. Chem. Theory Comput.* **2013**, *9*, 4064–4073.
3. Cattenacci, G.; Aschi, M.; Graziano, G.; Amadei, A. A theoretical study on the spectral and electrochemical properties of Ferrocene in different solvents. *Inorg. Chim. Acta* **2013**, *407*, 82–90.
4. Scott, D.R.; Becker, R.S. Comprehensive Investigation of the Electronic Spectroscopy and Theoretical Treatments of Ferrocene and Nickelocene. *J. Chem. Phys.* **1961**, *35*, 516–531.
5. Richer, G.; Sandorfy, C. The Far-Ultraviolet Absorption Spectra of ferrocene, cobaltocene and nickelocene. *J. Mol. Struct. THEOCHEM* **1985**, *123*, 317–327.
6. Harmon-Welch, G.E.; Hoefler, J.C.; Trujillo, M.R.; Bhuvanesh, N.; Bakhmutov, V.I.; Blümel, J. Creating Solid Solutions of Metallocenes: Migration of Nickelocene into the Ferrocene Crystal Lattice in the Absence of a Solvent. *J. Phys. Chem. C* **2023**, *127*, 3059–3066.
7. Trivedi, R.; Bhattacharyya, P. A theoretical study of ferrocene based on combined configuration interaction singles (CIS) and time-dependent density functional theory (TDDFT) approach. *Phys. Scr.* **2024**, *99*, 015929.
8. Zhao, H.; Pan, Y.; Lau, K.-C. Ferrocene/ferrocenium, cobaltocene/cobaltocenium and nickelocene/nickelocenium: from gas phase ionization energy to one-electron reduction potential in solvated medium. *Phys. Chem. Chem. Phys.* **2023**, *25*, 16921–16929.
9. Kamlesh; Aggarwal, P.; Mudgal, M.; Srivastava, A.K.; Raizada, P.; Singh, P.; Paul, A.; Singh, A. Electrochemistry of Nickelocene-Ferrocene Organometallic Complexes for Electrodeposition of Nickel-Iron-Based Nanostructured Film under Ambient Conditions for Oxygen Evolution Reaction. *ACS Appl. Nano Mater.* **2024**, *7*, 24455–24468.

10. Khan, G. Comparative Study of Molecular Orbitals of Cobaltocene and Nickelocene Based on Molecular Mechanics. *Arch. Appl. Sci. Res.* **2011**, *3*, 297–310.
11. Astruc, D. Why is Ferrocene so Exceptional? *Eur. J. Inorg. Chem.* **2017**, *1*, 6–29.
12. Noviadri, I.; Brown, K.N.; Fleming, D.S.; Gulyas, P.T.; Lay, P.A.; Masters, A.F.; Phillips, L. The Decamethylferrocenium/Decamethylferrocene Redox Couple: A Superior Redox Standard to the Ferrocenium/Ferrocene Redox Couple for Studying Solvent Effects on the Thermodynamics of Electron Transfer. *J. Phys. Chem. B* **1999**, *103*, 6713.
13. Sohn, Y.S.; Hendrickson, D.N.; Gray, H.B. Electronic structure of metallocenes. *J. Am. Chem. Soc.* **1971**, *93*, 3603–3612.
14. Elschenbroich, C. *Organometallics*, 3rd ed.; Wiley-VCH: Hoboken, NJ, USA, 2006; pp. 133–135.
15. Fronzoni, G.; Stener, M.; Furlan, S.; Decleva, P. Theoretical study of the photoionization shape resonances of cobaltocene and nickelocene. *Chem. Phys.* **2001**, *273*, 117–133.
16. Woldeamanuale, T.B. Density Functional Study of Molecular Orbitals of Cobaltocene and Nickelocene Molecules. *Arch. Chem. Res.* **2016**, *1*, 1–11.
17. Makoś, M.Z.; Gurunathan, P.K.; Raugei, S.; Kowalski, K.; Glezakou, V.A.; Rousseau, R. Modeling Absolute Redox Potentials of Ferrocene in the Condensed Phase. *J. Phys. Chem. Lett.* **2022**, *13*, 10005–10010.
18. Rudshiteyn, B.; Weber, J.L.; Coskun, D.; Devlaminck, P.A.; Zhang, S.; Reichman, D.R.; Shee, J.; Friesner, R.A. Calculation of Metallocene Ionization potentials via Auxiliary Field Quantum Monte Carlo: Toward Benchmark Quantum Chemistry for Transition Metals. *J. Chem. Theory Comput.* **2022**, *18*, 2845–2862.
19. NIST Chemistry WebBook. Available online: <https://webbook.nist.gov/> (accessed on 12 October 2025).
20. Ryan, M.F.; Eyler, J.R.; Richardson, D.E. Adiabatic ionization energies, bond disruption enthalpies, and solvation free energies for gas-phase metallocenes and metallocenium ions. *J. Am. Chem. Soc.* **1992**, *114*, 8611–8619.
21. Barfuss, S.; Emrich, R.-H.; Hirschwald, W.; Dowben, P.A.; Boag, N.M. A mass spectrometric investigation of chloro-, bromo- and methyl-ferrocenes by electron and photon impact ionisation. *J. Org. Chem.* **1990**, *391*, 209.
22. Aðalsteinsson, H.M.; Björnsson, R. Ionization energies of metallocenes: A coupled cluster study of cobaltocene. *Phys. Chem. Chem. Phys.* **2023**, *25*, 4570–4587.
23. Richardson, D.E. *Organometallic Ion Chemistry*; Kluwer Academic Publishers: Dordrecht, Netherlands, 1996; pp. 259–282.
24. Ryan, M.F.; Richardson, D.E.; Lichtenberger, D.L.; Gruhn, N.E. Gas Phase Ionization Energetics, Electron-Transfer Kinetics, and Ion Solvation Thermochemistry of Decamethylmetallocenes, Chromocene, and Cobaltocene. *Organometallics* **1994**, *13*, 1190–1199.
25. Begun, G.M.; Compton, R.N. Electron impact ionization studies of ferrocene, cobaltocene, nickelocene, and magnesocene. *J. Chem. Phys.* **1973**, *58*, 2271.
26. Tzeliou, C.E.; Zois, K.-P.; Tzeli, D. Molecular logic gates based on Ferrocene-Containing Compounds. *Inorganics* **2024**, *12*, 106.
27. He, F.; Zois, K.-P.; Tzeli, D.; Danopoulos, A.A.; Braunstein, P. N-Heterocyclic Carbenes as Bridgehead Donors in Metal Pincer Complexes. *Coord. Chem. Rev.* **2024**, *514*, 215757.
28. Papamichalis, E.; Petsalakis, I.D.; Tzeli, D. Tuning the photophysical properties of Nickel and Zinc Complexes of N-confused Tetraphenylporphyrin via trans-cis isomerization. *J. Phys. Chem. A* **2025**, *129*, 5942.
29. Adamo, C.; Barone, V. Toward reliable density functional methods without adjustable parameters: The PBE0 model. *J. Chem. Phys.* **1999**, *110*, 6158–6170.
30. Perdew, J.P.; Burke, K.; Ernzerhof, M. Generalized Gradient Approximation Made Simple. *Phys. Rev. Lett.* **1996**, *77*, 3865–3868.
31. Ernzerhof, M.; Scuseria, G.E. Assessment of the Perdew–Burke–Ernzerhof exchange–correlation functional. *J. Chem. Phys.* **1999**, *110*, 5029–5036.
32. Tao, J.; Perdew, J.P.; Staroverov, V.N.; Scuseria, G.E. Climbing the Density Functional Ladder: Nonempirical Meta-Generalized Gradient Approximation Designed for Molecules and Solids. *Phys. Rev. Lett.* **2003**, *91*, 146401.
33. Jensen, K.P. Bioinorganic Chemistry Modeled with the TPSSh Density Functional. *Inorg. Chem.* **2008**, *47*, 10357–10365.
34. Chai, J.-D.; Head-Gordon, M. Long-range corrected hybrid density functionals with damped atom-atom dispersion corrections. *Phys. Chem. Chem. Phys.* **2008**, *10*, 6615–6620.
35. Hehre, W.J.; Ditchfield, R.; Pople, J.A. Self-Consistent Molecular Orbital Methods. XII. Further Extensions of Gaussian-Type Basis Sets for Use in Molecular Orbital Studies of Organic Molecules. *J. Chem. Phys.* **1972**, *56*, 2257–2261.
36. Weigend, F.; Ahlrichs, R. Balanced basis sets of split valence, triple zeta valence and quadruple zeta valence quality for H to Rn: Design and assessment of accuracy. *Phys. Chem. Chem. Phys.* **2005**, *7*, 3297–3305.
37. Guido, C.A.; Brémond, E.; Adamo, C.; Cortona, P. Communication: One third: A new recipe for the PBE0 paradigm. *J. Chem. Phys.* **2013**, *138*, 021104.

38. Morgante, P.; Peverati, R. Comparison of the Performance of Density Functional Methods for the Description of Spin States and Binding Energies of Porphyrins. *Molecules* **2023**, *28*, 3487.
39. Tzeliou, C.E.; Tzeli, D. 3-Input AND Molecular Logic Gate with Enhanced Fluorescence Output: The Key Atom for the Accurate Prediction of the Spectra. *J. Chem. Inf. Model.* **2022**, *62*, 6436–6448.
40. Tzeliou, C.E.; Tzeli, D. Metallocene-Naphthalimide Derivatives: The Effect of Geometry, DFT Methodology, and Transition Metals on Absorption Spectra. *Molecules* **2023**, *28*, 3565.
41. Scerri, G.J.; Spiteri, J.C.; Mallia, C.J.; Magri, D.C. A lab-on-a-molecule with an enhanced fluorescent readout on detection of three chemical species. *Chem. Commun.* **2019**, *55*, 4961–4964.
42. Scuseria, G.E.; Scheiner, A.C.; Lee, T.J.; Rice, J.E.; Schaefer, H.F., III. The closed-shell coupled cluster single and double excitation (CCSD) model for the description of electron correlation. A comparison with configuration interaction (CISD) results. *J. Chem. Phys.* **1987**, *86*, 2881–2890.
43. Paulechka, E.; Kazakov, A. Efficient DLPNO–CCSD(T)-Based Estimation of Formation Enthalpies for C-, H-, O-, and N-Containing Closed-Shell Compounds Validated Against Critically Evaluated Experimental Data. *J. Phys. Chem. A* **2017**, *121*, 4379–4387.
44. Kreplin, A.; Knowles, P.J.; Werner, H.-J. Second-order MCSCF optimization revisited. I. Improved algorithms for fast and robust second-order CASSCF convergence. *J. Chem. Phys.* **2019**, *150*, 194106.
45. Angeli, C.; Cimiraglia, R.; Evangelisti, S.; Leininger, T.; Malrieu, J.P. Introduction of n-electron valence states for multireference perturbation theory. *J. Chem. Phys.* **2001**, *114*, 10252–10264.
46. Angeli, C.; Cimiraglia, R.; Malrieu, J.P. N-electron valence state perturbation theory: A fast implementation of the strongly contracted variant. *Chem. Phys. Lett.* **2001**, *350*, 297–305.
47. Tzeli, D.; Matoušek, M.; Brabec, J.; Pernal, K.; Golub, P.; Veis, L.; Raugei, S.; Xantheas, S.S. The importance of electron correlation on the geometry and electronic structure of [2Fe-2S] systems: A benchmark study of the [Fe₂S₂(SCH₃)₄]₂-,₃-,₄- [Fe₂S₂(SCys)₄]₂-, [Fe₂S₂(S-p-tol)₄]₂-, and [Fe₂S₂(S-o-xy)₄]₂- complexes. *J. Chem. Theory Comput.* **2024**, *20*, 10406.
48. Mejuto-Zaera, C.; Tzeli, D.; Williams-Young, D.; Tubman, N.M.; Matoušek, M.; Brabec, J.; Veis, L.; Xantheas, S.S.; de Jong, W.A. The Effect of Geometry, Spin and Orbital Optimization in Achieving Accurate, Correlated Results for Iron-Sulfur Cubanes. *J. Chem. Theory Comput.* **2022**, *18*, 687–702.
49. Tzeli, D.; Raugei, S.; Xantheas, S.S. Quantitative Account of the Bonding Properties of a Rubredoxin Model Complex [Fe(SCH₃)₄]_q, q = -2, -1, +2, +3. *J. Chem. Theory Comput.* **2021**, *17*, 6080–6091.
50. Chamkin, A.A.; Serkova, E.S. DFT, DLPNO-CCSD(T), and NEVPT2 benchmark study of the reaction between ferrocenium and trimethylphosphine. *J. Comput. Chem.* **2020**, *41*, 2388–2397.
51. Musgrave, R.A.; Russell, A.D.; Gamm, P.R.; Hailes, R.L.N.; Lam, K.; Sparkes, H.A.; Green, J.C.; Geiger, W.E.; Manners, I. Redox Chemistry of Nickelocene-Based Monomers and Polymers. *Organometallics* **2021**, *40*, 1945–1955.
52. Ribeiro, R.B.; Varella, M.T.d.N. Excited state properties of an A–D–A non-fullerene electron acceptor: A LC-TD-DFTB study. *Phys. Chem. Chem. Phys.* **2024**, *26*, 12993–13005.
53. Xue, Y.; Dou, Y.; An, L.; Zheng, Y.; Zhang, L.; Liu, Y. Electronic structure and spectral properties of aurones as visible range fluorescent probes: A DFT/TDDFT study. *RSC Adv.* **2016**, *6*, 7002–7010.
54. Shao, Y.; Mei, Y.; Sundholm, D.; Kaila, V.R.I. Benchmarking the Performance of Time-Dependent Density Functional Theory Methods on Biochromophores. *J. Chem. Theory Comput.* **2020**, *16*, 587–600.
55. Kolokytha, C.; Sinani, A.; Manouras, T.; Angelakos, E.; Argitis, P.; Lathiotakis, N.N.; Riziotis, C.; Tzeli, D. Photophysical Investigation of Dyes and Dye-PMMA Systems: Insights into Absorption, Emission, and Charge Transfer Mechanisms. *J. Phys. Chem. A* **2025**, *129*, 1219–1232.
56. Caricato, M.; Mennucci, B.; Tomasi, J.; Ingrosso, F.; Cammi, R.; Corni, S.; Scalmani, G. Formation and relaxation of excited states in solution: A new time dependent polarizable continuum model based on time dependent density functional theory. *J. Chem. Phys.* **2006**, *124*, 124520.
57. Cicolella, A.; Romano, E.; Barone, V.; De Rosa, C.; Talarico, G. Metallocenes and beyond for propene polymerization: energy decomposition of density functional computations unravels the different interplay of stereoelectronic effects. *Organometallics* **2022**, *41*, 3872–3883.
58. Kendall, R.A.; Dunning, T.H., Jr.; Harrison, R.J. Electron affinities of the first-row atoms revisited. Systematic basis sets and wave functions. *J. Chem. Phys.* **1992**, *96*, 6796–6806.
59. Frisch, M.J.; Trucks, G.W.; Schlegel, H.B.; Scuseria, G.E.; Robb, M.A.; Cheeseman, J.R.; Scalmani, G.; Barone, V.; Mennucci, B.; Petersson, G.A. et al. *Gaussian*, version 16, revision C.01; Gaussian, Inc.: Walingford, CT, USA, 2016.

60. Neese, F. The ORCA program system, *Wiley Interdiscip. Rev. Comput. Mol. Sci.* **2012**, *2*, 73–78.
61. Neese, F. Software update: The ORCA program system—Version 6.0. *Wiley Interdiscip. Rev. Comput. Mol. Sci.* **2025**, *15*, e70019.

Disclaimer/Publisher's Note: The statements, opinions and data contained in all publications are solely those of the individual author(s) and contributor(s) and not of MDPI and/or the editor(s). MDPI and/or the editor(s) disclaim responsibility for any injury to people or property resulting from any ideas, methods, instructions or products referred to in the content.